Homogenic endothelium-independent hematopoiesis ensures the abundance of erythrocytes and macrophages during zebrafish development.

Ramy Elsaid[1,*], Aya Mikdache[1], Keinis Quintero Castillo[2], Yazan Salloum[1], Patricia Diabangouaya[1,#], Gwendoline Gros[1,#], Carmen G. Feijoo[2] and Pedro P. Hernández[1,*].

[1]Institut Curie, PSL Research University CNRS UMR 3215, INSERM U934, 26 Rue d'Ulm, 75248 Paris Cedex 05, France.
[2]Fish Immunology Laboratory, Faculty of Life Science, Andres Bello University, 8370146 Santiago, Chile.

# These authors contributed equally to this work.

[*]Corresponding author. Email: pedro.hernandez-cerda@curie.fr (P.P.H.) and ramy.elsaid@curie.fr (R.E.).

Short running title: Layered erythromyeloid ontogeny in zebrafish.

Abstract

In all organisms studied, from flies to humans, blood cells emerge in several sequential waves and from distinct hematopoietic origins. However, the relative contribution of these ontogenetically distinct hematopoietic waves to embryonic blood lineages and to tissue regeneration during development is yet elusive. Here, using a lineage-specific 'switch and trace' strategy in the zebrafish embryo, we report that the definitive hematopoietic progeny barely contributes to erythrocytes and macrophages during early development. Lineage tracing further show that ontogenetically distinct macrophages exhibit differential recruitment to the site of injury based on the developmental stage of the organism. We further demonstrate that primitive macrophages can solely maintain tissue regeneration during early larval developmental stages after selective ablation of definitive macrophages. Our findings highlight that the sequential emergence of hematopoietic waves in embryos ensures the abundance of blood cells required for tissue homeostasis and integrity during development.

Keywords

Ontogeny; Hematopoiesis; Lineage tracing; Regeneration; Zebrafish

Introduction

Hematopoiesis is a complex biological process by which all mature blood lineages are generated. In mammals, hematopoiesis originates from distinct blood progenitors that emerge during development through an endothelial-to-hematopoietic transition mechanism (EHT) [1–3], resulting in a layered organization of the immune system [4]. As in mammals, zebrafish hematopoiesis also consists of multiple waves that emerge at distinct anatomical locations [4]. In the zebrafish embryo, primitive hematopoiesis emerges intra-embryonically directly from mesoderm around 11 hours post-fertilization (hpf) in the rostral blood island (RBI) and the posterior lateral mesoderm (PLM) and generates primitive erythrocytes and myeloid cells [4,5]. Other definitive or endothelial-derived hematopoietic waves are also produced in the developing organism [4]. One of them is a transient wave that emerges from the posterior blood island (PBI) at 24-30 hpf via EHT and gives rise to erythro-myeloid progenitors (EMPs) like those in mammals [6–8]. At 36 hpf, other waves of HSCs and HSC-independent progenitors emerge from the dorsal aorta (DA) via EHT [1,3]. These DA-derived hematopoietic progenitors then migrate to the caudal hematopoietic tissue (CHT), the fetal liver counterpart in zebrafish [9]. Therefore, due to its similarity to mammalian hematopoiesis, the zebrafish is an excellent model to study the ontogeny of different hematopoietic waves during development.

Although it is well characterized that blood cells are produced in sequential and overlapping waves [4], little is known about their contribution to different hematopoietic lineages during development. Recently, independent reports support the notion that definitive hematopoiesis sustains embryonic blood lineages [8,10–12]. However, primitive hematopoietic progenitors give rise also to the erythromyeloid lineage and it is yet unknown to what extent

103 these progenitors contribute to embryonic blood lineages. This is mainly due to the lack of
104 specific markers for primitive hematopoietic progenitors in mammals [4,7,13,14].

105 The difficulty in accurately tracing the output of each wave in mammalian animal models has
106 hindered the full understanding of immune cell ontogeny. In this study, we used the unique
107 strengths of the zebrafish embryo to perform temporarily resolved lineage tracing combined
108 with live imaging to investigate the embryonic erythromyeloid lineage ontogeny *in vivo*. We
109 unveiled that embryonic erythromyeloid lineages originate from primitive hematopoietic
110 progenitors with a delayed contribution from definitive hematopoietic waves to the
111 erythromyeloid lineage till the larval developmental stage. We further showed that primitive
112 macrophages were recruited to the damage site earlier than their definitive counterparts. Our
113 results also suggest that primitive macrophages maintain tissue regeneration during early
114 larval developmental stages after selective ablation of definitive macrophages. Combined,
115 our study reveals that the sequential emergence of hematopoietic waves ensures the
116 abundance of macrophages and erythrocytes required for tissue homeostasis and integrity
117 during development.

118

119

120

121

122

123

124

125

126 Results

127 Primitive hematopoietic progenitors sustain erythrocytes during embryonic development.

128 As all definitive hematopoietic progenitors originate from hemogenic endothelium (HE) as
129 early as 24 hpf [1,6,8,10,15,16], while primitive progenitors originate directly from mesoderm in
130 zebrafish[1,3,17,18], we set up a strategy to distinguish between primitive and definitive
131 hematopoietic progenitors based on their tissue of origin. We used the endothelial-specific
132 tamoxifen-inducible transgenic line *Tg(fli1a:CreERT2)* [19] in combination with different
133 hematopoietic lineage-specific switch and trace lines[20]. Our inducible labeling strategy at 24
134 hpf will label exclusively definitive hematopoietic progenitors as they emerge from the HE
135 without labeling primitive hematopoietic progenitors. To assess the efficiency of our labeling
136 strategy, we combined the *Tg(fli1a:CreERT2)* line with two different independent transgenic
137 lines, the lymphocyte-specific *Tg(lck:loxP-DsRedx-loxP-GFP)* [8,21] line (supplemental Figure 1A)
138 and the *Tg(coro1a:loxP-DsRedx-loxP-GFP)* line which labels all leukocytes[13,22] (supplemental
139 Figure 1D). We found that 80% of thymocytes in the thymus, which have only a definitive
140 hematopoietic origin [8,23], were labelled using either the *Tg(lck:loxP-DsRedx-loxP-GFP)*
141 (supplemental Figure 1B-C) or the *Tg(coro1a:loxP-DsRedx-loxP-GFP)* lines (supplemental
142 Figure 1E-F), indicating the high labelling efficiency of our system.

143 To determine the origin of erythrocytes during embryonic development and early larval
144 stages, we combined the *Tg(fli1a:CreERT2)* line with the erythrocyte-specific *Tg(α/β_{a2}-*
145 *globin:loxP-DsRedx-loxP-GFP)* line (referred to hereafter as globin:switch) [8,18]. In double
146 transgenic zebrafish, 4-OH-tamoxifen (4-OHT) induces cre recombination and removes the
147 DsRed cassette, leading to permanent GFP expression in *fli1a*$^{+}$-derived erythroid progeny
148 (Figure 1A). To determine the contribution of definitive hematopoietic progenitors to

149 erythropoiesis during early stages of development, we exposed embryos to either 4-OHT or
150 ethanol (EtOH) starting at 24 hpf to label the aortic-endothelium-derived definitive
151 hematopoietic progenitors [1,8,15], and then monitored GFP$^+$ definitive erythrocytes via live
152 imaging (Figure 1B and supplemental video 1). Primitive hematopoietic progenitors robustly
153 generated erythrocytes from early embryonic stages (Figure 1B). In contrast, GFP$^+$ definitive
154 erythrocytes started to emerge after 2 dpf, accumulated in the CHT region starting at 4 dpf
155 (Figure 1C) and their contribution to the erythrocyte pool was not appreciable until later larval
156 developmental stages (~12 dpf, Figure 1C-F).

157 These results indicate that erythrocytes emerge in a layered organization during embryonic
158 and early larval stages as in mammals [24], and that primitive hematopoietic progenitors
159 generate a sufficient number of erythrocytes to sustain embryonic survival and tissue
160 homeostasis [25].

161 Embryonic macrophages originate exclusively from primitive hematopoietic progenitors.

162 To assess the contribution of definitive hematopoietic progenitors to the embryonic
163 macrophage pool, we marked the latter by combining the *Tg(fli1a:CreERT2)* line with the
164 macrophage-specific *Tg(mpeg1:LoxP-DsRedx-LoxP-GFP-NTR)* line (referred to hereafter as
165 mpeg1:switch) [26,27]. As aforementioned, 4-OHT-induced cre recombination leads to
166 permanent GFP expression in *fli1a*$^+$-derived macrophages progeny (Figure 2A). Using this
167 system, embryonic microglia cells, which are known to be of primitive hematopoietic origin
168 in zebrafish [7,13], were not labelled, indicating the precision of this labelling system
169 (supplemental figure 2A-B). While primitive macrophages contributed robustly to the
170 embryonic macrophage pool, we found that definitive hematopoietic progenitors minimally

171 contribute to macrophages during early developmental stages, akin to erythrocytes ontogeny
172 (Figure 2B). We showed further that GFP$^+$ definitive macrophages started to emerge after 2
173 dpf and gradually increased in numbers in the CHT region (Figure 2B and E) with a delayed
174 modest contribution to the macrophage pool in the periphery starting after 4 dpf (Figure 2B-
175 D). GFP$^+$ definitive macrophages contributed robustly to peripheral macrophages by 16 dpf,
176 suggesting a distinct differentiation kinetics of primitive and definitive macrophages
177 throughout development (Figure 2C).

178 Altogether, our lineage tracing experiments show that aortic endothelium derived
179 hematopoietic progenitors are barely contributing to embryonic erythroid and myeloid
180 lineages (Figures 1 and 2).

181 Ontogenically distinct macrophages are differentially recruited to the site of injury.

182 It has been recently reported that distinct macrophage subpopulations play different roles to
183 promote tail regeneration after amputation [28,29]. However, whether ontogenetically distinct
184 macrophages display different functions and recruitment behaviors to the site of injury
185 remains poorly understood. Therefore, we sought to analyze if macrophages of distinct
186 origins are recruited in a differential manner to the damage site at different developmental
187 stages. Using the same labelling strategy (Figure 2A), we analyzed macrophages recruitment
188 to the damaged site in embryos (2 dpf) and larvae (5 dpf) since our lineage tracing
189 experiments showed a different abundance of ontogenetically distinct macrophages at these
190 developmental stages (Figure 2). In embryos, we observed that primitive macrophages were
191 recruited to the site of injury at 24 hours post amputation (hpa) and 48 hpa (Figure 3A-B and
192 supplemental Figure 3A). We then analyzed macrophage recruitment to the damage site in
193 larvae, where both primitive and definitive macrophage populations coexist in the periphery.

194 We did not observe differences in the recruitment of both primitive and definitive
195 macrophages to the damage site 24 hpa with a slight increase in the number of definitive
196 macrophages 48 hpa (Figure 3C, E and supplemental Figure 3B). Altogether, these results
197 suggest that primitive macrophages can alone modulate tail fin regeneration during
198 embryonic stages while both macrophage populations are recruited to the damaged site in
199 the larvae.
200 Previous reports showed that the first recruited macrophages play an important role in
201 proper tail fin regeneration [29–31], therefore, we further analyzed which macrophage
202 population is recruited first to the site of injury. We found that primitive macrophages are
203 recruited earlier than their definitive counterparts showed by the reduced number of
204 definitive macrophages recruited to the site of injury from 3 to 12 hpa (Figure 3E-F). In
205 addition, primitive macrophages manifested sings of active phagocytosis activity as early as 3
206 hpa evidenced by the appearance of vacuoles in their cell bodies (Figure 3D). Since our
207 observation of a delay in the recruitment of definitive macrophages could be the result of
208 differences in the number of primitive and definitive macrophages in the periphery at the
209 time of injury, we attempted to normalize their numbers. Data was normalized by dividing
210 the number of each recruited macrophage subpopulation by their total number in the tail of
211 the same larvae [29]. After normalization, we still observed that primitive macrophages are
212 recruited earlier compared to their definitive counterparts with a reduced recruitment of
213 definitive macrophages at 3, 6 and 12 hpa, when compared to their primitive counterparts
214 (Figure 3F). These data indicate that primitive macrophages, as the first arrivals to the damage
215 site, may have a specific role in the regeneration process after amputation during
216 development.
217

218 Selective ablation of definitive macrophages does not impair tail fin regeneration during early
219 larval developmental stages.
220 To evaluate the contribution of ontogenetically distinct macrophages to tail fin regeneration,
221 we used the mpeg1 switch line *Tg(mpeg1:loxP-dsRed-loxP-eGFP-NTR)* that allows selective
222 ablation of macrophages based on their origin. In this line, the expression of bacterial
223 nitroreductase (NTR) is under the control of the *mpeg1* promoter [27]. Thus, the NTR will be
224 expressed exclusively in the traced macrophages, thereby, traced macrophages could be
225 ablated by metronidazole (MTZ) treatment [32] (Figure 4A). To assess the efficiency of the NTR-
226 MTZ system, we quantified the number of primitive and definitive macrophages in the tail
227 after treatment with either DMSO or MTZ for 48 hours from 4 to 6 dpf. We found that while
228 primitive macrophages were not affected by the MTZ treatment, definitive macrophages
229 were significantly reduced after 48 hours of MTZ treatment (Supplemental Figure 3C-D).
230 We next performed tail fin amputation in 5 dpf larvae that was treated with either DMSO or
231 MTZ from 4-6 dpf to ensure ablation of definitive macrophages through the regeneration
232 process. While primitive macrophage numbers and recruitment were not affected during the
233 regeneration process, definitive macrophages were significantly reduced during the first 48
234 hpa but recovered by 72 hpa (Figure 4B-E and supplemental Figure 3E). Next, we analyzed
235 macrophage recruitment to the site of injury in MTZ-treated larvae from 24 to 72 hpa. We
236 normalized the number of recruited macrophages by the number of total macrophages in the
237 tail at their respective timepoints and we observed a decrease in the number of recruited
238 definitive macrophages during the first 48 hpa, indicating the efficiency of the MTZ-mediated
239 selective ablation of definitive macrophages (Figure 4F). We then performed tail fin
240 regeneration analysis and observed no differences in the regenerated tail fin area between
241 larvae treated with either DMSO or MTZ (Figure 4G-H). Furthermore, cell proliferation was

242 not altered in the regenerated tail of 72 hpa larvae with either DMSO or MTZ (Supplemental
243 Figure 3F-G).
244 To determine if this observation could be replicated in the absence of definitive macrophages,
245 we analyzed tail fin regeneration in *cmyb*-deficient zebrafish that lack HSCs, have impaired
246 definitive hematopoiesis and have reduced numbers of definitive macrophages[7,33,34]. We
247 found no differences in regeneration efficiency, measured by the tail fin area, between *cmyb*-
248 deficient and wild type larvae (Figure 4I-J). Our results, thus, indicate that primitive
249 macrophages recruitment to the damage site is not affected and tail fin regeneration is not
250 impaired when definitive macrophages are depleted.

251 Depletion of primitive macrophages impairs tail fin regeneration in early larvae.

252 To characterize the role of primitive macrophages in tail fin regeneration during early larval
253 developmental stages, we chemically depleted them at 48 hpf, before the maturation of their
254 definitive counterparts as previously reported in zebrafish[35] (Figure 5A). In line with previous
255 studies[29,30,35], intravenous injection of L-clodronate at 48 hpf efficiently depleted
256 macrophages in 5 dpf zebrafish larvae (Figure 5B-C). Thus, we performed tail fin amputation
257 and regeneration analysis in L-clodronate injected larvae and compared them with L-PBS
258 injected controls (Figure 5D-E). We found fewer macrophages at the injury site in L-clodronate
259 injected fish compared to L-PBS injected controls (Figure 5F), suggesting primitive
260 macrophage ablation at 72 and 120 hpa. In contrast to the selective ablation of definitive
261 macrophages (Figure 4), depletion of primitive macrophages impaired tail fin regeneration,
262 as measured by the tail fin area, at 72 hpa and 120 hpa (Figure 5D-E). These observations
263 suggest that primitive macrophage depletion leads to tail fin regeneration defects,
264 highlighting the functional differences among macrophages based on their ontogeny. Overall,

265 these results shed light on the critical role of early-recruited primitive macrophages during
266 tail fin regeneration in early zebrafish larvae.
267
268 Discussion
269 Two major waves of hematopoietic progenitors are generated during embryogenesis: the
270 primitive and the definitive waves. Both waves generate erythromyeloid progenitors during
271 embryogenesis, however, having a dual source of blood progenitors makes it difficult to
272 assess accurately each wave contribution to blood lineages in homeostasis and upon tissue
273 injury. Therefore, the lack of specific markers to identify different populations from the same
274 blood lineage according to their origin and function has hindered the full understanding of
275 immune cell ontogeny.
276 Here, we classified hematopoietic waves according to their site of origin and tracked them
277 during homeostasis and upon recruitment to the site of injury. Our study shows that the
278 hematopoietic system follows a layered strategy to provide a timely supply of innate immune
279 cells and erythrocytes. Under steady-state conditions, we found that the contribution of
280 definitive hematopoietic progenitors to embryonic erythromyeloid lineage is limited. This is
281 of particular interest as none of the lineage tracing strategies performed in mice, despite their
282 elegant designs, are specific to definitive hematopoietic waves. Our results also complement
283 the recently reported observations that HSCs have a delayed contribution to the
284 lymphomyeloid lineage during development [10].
285 In addition, as timely recruitment of macrophages to the damage site is important to ensure
286 proper tail fin regeneration [28–31], we found that the primitive macrophages are the first
287 responders after tail fin injury showed by their active phagocytic activity as early as 3 hpa and
288 their earlier recruitment than their definitive counterparts. The difference in recruitment

behaviour between primitive and definitive macrophages could be due to that the primitive macrophages are more sensitive to damage sensing and/or a consequence of the immaturity of definitive macrophages at early developmental stages. However, we delineated that definitive macrophages regenerate following their depletion but are not required for tail regeneration during early developmental stages. These intriguing results suggest that embryos and early larvae adopt a layered ontogeny of macrophages to ensure their abundance for a timely contribution to tissue regeneration. Further studies are needed to determine the molecular signatures of these ontogenetically distinct populations accounting for their different behaviors.

A significant discovery from our study highlights the key role of primitive macrophages in orchestrating tissue regeneration. Depletion of primitive macrophages during early developmental stages had a negative impact on the regeneration of tail fins. In contrast, the selective ablation of definitive macrophages did not hinder tail fin regeneration. This conclusion is supported by additional experiments, where we independently targeted either the definitive or primitive macrophage populations using two distinct methods and then analyzed the regrowth of tail fins in amputated larvae. These results underscore the remarkable capacity of primitive macrophages to facilitate timely tissue regeneration.

In conclusion, our study provides insights into the ontogeny of the erythromyeloid lineage during embryonic/early larval developmental stages. Our findings support the notion that embryos show a sequential emergence of hematopoietic waves to ensure the abundance of macrophages required for tissue homeostasis and regeneration during a crucial developmental time window. In line with our results, it has been recently reported in mice [11,36–38] and in zebrafish [8,10] that embryonic and adult HSCs do not give rise to several blood subtypes at steady state, upon ablation of mature blood cells, and in response to immune

313 challenge. These observations indicate that ensuring a rapid response to stress to maintain
314 tissue homeostasis in an HSC-independent manner might be a conserved mechanism
315 between species throughout their life.

316 **Limitations of the study**

317 *fli1a* is expressed in mature thrombocytes[39] and is expressed also at 10 hpf in the lateral
318 mesoderm[40].Therefore, we used an inducible system to label all definitive hematopoietic
319 progenitors as they emerge from hemogenic endothelium at 24 hpf. Using our labeling
320 strategy, we could not distinguish distinct definitive hematopoietic progenitors as they all
321 share the expression of *fli1a*$^{+}$ as they go through EHT[1,3,10],therefore, better tools are required.
322 Furthermore, in our study we were not able to selectively ablate the primitive macrophage
323 population because of lacking a specific marker to the primitive hematopoietic progenitors
324 and their progeny. In addition, we were unable to guarantee that all definitive hematopoietic
325 progenitors were successfully labeled. According to the tracing result that ~80% of
326 thymocytes were labeled, there is still a remaining ~20% of cells that likely derived from
327 unlabeled definitive progenitors due to the incomplete *loxP* recombination.

328
329
330
331
332
333
334
335
336
337
338
339
340
341
342
343
344

345 **STAR★Methods**

346 **Key resources table**

REAGENT or RESOURCE	SOURCE	IDENTIFIER
Chemicals, peptides, and recombinant proteins		
(Z)-4-Hydroxytamoxifen (4-OHT)	Sigma	Cat# H7904
Ethyl 3-aminobenzoate methane sulfonate salt (Tricaine)	Sigma	Cat# A5040
Dimethyl sulfoxide (DMSO)	Sigma	Cat# D5879
Metronidazole (MTZ)	Sigma	Cat# M1547
5-ethynyl-2'-deoxyuridine (EdU)	ThermoFisher SCIENTIFIC	Cat # C10340
L-clodronate	LIPOSOMA	www.clodronateliposomes.org
Experimental models: Organisms/strains		
Zebrafish *Tg(fli1a: CreER^{T2})*	Sánchez-Iranzo et al., 2018[19]	ZFIN: ZDBTGCONSTRCT-170711-8
Zebrafish *Tg(mpeg1:LoxP-DsRedx-LoxP-GFP-NTR)*	Lin et al., 2019[26]	ZFIN: ZDB-ALT-191122-8
Tg(coro1a:loxP-DsRedx-loxP-GFP)	Xu et al., 2015[13]	ZFIN: ZDB-TGCONSTRCT-160114-1
Tg(globin:loxP-DsRedx-loxP-GFP)	Tian et al., 2017[8]	ZFIN: ZDB-TGCONSTRCT-180702-2
Tg(lck:loxP-DsRedx-loxP-GFP)	Tian et al., 2017[8]	ZFIN: ZDB-TGCONSTRCT-180702-3
Tg(cmyb$^{+/-}$;kdrl:Cre^{+}; ßactin:Switch-DsRed^{+})	Ferrero et al., 2018[7]	N/A
Software and algorithms		
ImageJ	Schneider et al.[7]	https://imagej.nih.gov/ij/
Prism 9	GraphPad	https://www.graphpad.com/

347

348 **Resource availability**

349 **Lead contact**

350 Further information and requests for scripts, resources, and reagents should be directed to
351 and will be fulfilled by lead contact, Pedro P. Hernández (pedro.hernandez-cerda@curie.fr).

352

353

354 **Materials and Data availability**

355 This study did not generate new unique reagents. The data sets generated during the
356 current study are available from the corresponding authors upon request.

357 **Experimental model and subject details**

358

359 **Zebrafish.** Embryonic and adult zebrafish (*Danio rerio*) were maintained at 28°C on a 14-hour
360 light/10-hour dark cycle. The collected embryos were raised in fish water containing
361 0.01% methylene blue to prevent fungal growth. All fish are housed in the fish facility of our
362 laboratory, which was built according to the local animal welfare standards. Animal care and
363 use for this study were performed in accordance with the recommendations of the European
364 Community (2010/63/UE) for the care and use of laboratory animals. Experimental
365 procedures were specifically approved by the ethics committee of the Institut Curie CEEA-IC
366 #118 (Authorization number - APAFiS#21197-2019062521156746-v2 - given by National
367 Authority) in compliance with the international guidelines."

368 **Transgenic lines.** The following lines of the AB stain were used: *Tg(fli1a: CreER^{T2})*[19],
369 *Tg(mpeg1:LoxP-DsRedx-LoxP-GFP-NTR)*[26],*Tg(coro1a:loxP-DsRedx-loxP-GFP)*[13], *Tg(globin:loxP-*
370 *DsRedx-loxP-GFP)* [8], *Tg(lck:loxP-DsRedx-loxP-GFP)* [8] *and Tg(cmyb$^{+/-}$; kdrl:Cre^{+}; ßactin:Switch-*
371 *DsRed^{+})*[7] *cmyb*^{null} embryos were identified at 5 dpf based on the absence of HSC-derived
372 *DsRed^{+}* thymocytes.

373 **Methods details**

374

375 **Fluorescence Microscopy.** Zebrafish embryos, larvae and adults were anesthetized with
376 0.01% tricaine (A5040, Sigma) and mounted in 2.5% 2.5% methylcellulose in 35-mm imaging
377 dishes (MatTek) as described previously [41]. Fluorescent imaging was performed with either
378 Zeiss Axio Zoom V.16 upright microscope with an AxioCam HRm Zeiss camera and Zeiss Zen
379 3.3 software or with Leica thunder imaging system with Leica LAS-X software. Fluorescence
380 was detected with dsRed and green fluorescent protein (GFP) filters.
381

382 **Image Analysis.** All images were analyzed using FIJI software [42].
383

384 **CreER-loxP Cell Labelling (Lineage Tracing).** Zebrafish embryos at 24 hpf were treated with
385 5 µM 4-OHT (H7904, Sigma) for 24 hours. Controls were incubated in the equivalent amount
386 of Ethanol solution during the same period. Light exposure was avoided by using foil to cover
387 the plates as 4-OHT is light sensitive. After treatment, embryos were washed with fresh
388 embryo medium and placed back in incubator. From 5 dpf, larvae were transferred to the fish
389 facility nursery where they were kept and fed. Embryos were raised for further analysis at
390 different developmental stages.
391

392 **Macrophage ablation and drug treatments.** The *Tg(fli1CreER^{T2};mpeg1:loxP-DsRedx-loxP-*
393 *GFP-NTR)* embryos were immersed in system water containing 10 mM metronidazole
394 (M1547, Sigma) for 48 hours, which caused an acute depletion of GFP-NTR^{+} cells. The medium
395 containing the MTZ was changed every 24 hours. Controls were incubated in the equivalent

396 amount of DMSO solution during the same period. Light exposure was avoided by using foil
397 to cover the plates as MTZ is light sensitive. Zebrafish were further analyzed by fluorescence
398 imaging at different developmental time points. For primitive macrophage ablation using L-
399 clodronate injection, the larvae were anesthetized in 0.016% Tricaine and microinjected with
400 5 nl of liposome encapsulated clodronate (www.clodronateliposomes.org) in the posterior
401 caudal vein in the Urogenital Opening region at 48 hpf. Control embryos were similarly
402 injected with liposome-PBS (L-PBS).
403
404 **Tail Fin Amputation.** 2 and 5 dpf larvae were anesthetized with 0.01% tricaine and amputated
405 with a sterile scalpel. The amputation was performed by using the posterior section of the
406 ventral pigmentation gap in the tail fin as a reference, and immediately after amputation
407 larvae were incubated in either E3 medium, or in MTZ in case of macrophage ablation at 28°C.
408
409 **Quantification of Tail Fin Regeneration.** At 24-, 48- and 72-hours post amputation or dpa
410 (6,7- and 8-days post fertilization, respectively), larvae were mounted in 2.5%
411 methylcellulose, and regenerating tail fins were imaged in bright field. Tail fin area was
412 measured from the anterior section of the ventral tail fin gap to the end of the regenerating
413 fin, as previously described[43], using FiJi software. Tail fin areas were calculated and expressed
414 in square micrometers (um^2).
415
416 **Quantification of Tail Macrophages.** Macrophages were quantified based on their location in
417 the tail (periphery vs CHT) (Figure 2B) in non-amputated larvae. In amputated larvae,
418 recruited macrophages to the site of injury were quantified. Normalization of recruited
419 macrophage numbers was obtained by dividing the number of recruited macrophage
420 subpopulation by their total number in the tail of the same larvae (periphery, CHT and
421 recruited macrophages) [29]. We have factored the labelling efficiency in our quantification data
422 analysis in Figure 3 and Figure 4.
423
424 **Cell Proliferation analysis.** For cell proliferation analysis, EdU analysis was performed in 72
425 hpa larvae previously fixed in 4% PFA and dehydrated with methanol, using Click-iT EdU cell
426 proliferation kit for imaging, Alexa Fluor 647 dye. Stained larvae were imaged using
427 fluorescence microscopy and analyzed using FIJI.
428
429 **Quantification and statistical analysis.** Statistical analyses were performed by the GraphPad
430 Prism software (Prism 9). All experiments with only two groups and one dependent variable
431 were compared using an unpaired t-test with Welch's correction. Two-way ANOVA with
432 Sidak's multiple comparison was used for this analysis. Statistical data show mean ± s.e.m.
433 Each dot plot value represents an independent embryo, and every experiment was conducted
434 three times independently. The corrected total cell fluorescence (CTCF) was calculated using
435 the formula 'Integrated density whole – (area whole embryo x mean fluorescence
436 background)'. This formula is loosely based on a method described for calculating cell-
437 fluorescence [10]. To calculate the CTCF percentage for DsRed+ cells, the CTCF value of DsRed
438 was divided by the total summation of CTCF values for both DsRed and GFP in each larvae.
439 The same was done for calculating CTCF percentage for GFP+ cells.
440
441
442

Acknowledgments

We thank the Developmental Biology Curie imaging facility (PICT-IBiSA@BDD, Paris, France, UMR3215/U934) members of the France-BioImaging national research infrastructure for their help and advice. We also thank the members of the animal facility of Institut Curie for zebrafish care. We also thank Yohanns Bellaiche and all the members of the Hernandez lab for thoughtful and valuable discussions. We are grateful to Nadia Mercader for providing the *Tg(fli1a:CreERT2)*, we also thank Zilong Wen for providing all the immune and blood lineage switch lines used in this study. This work was supported by the Institut Curie, INSERM, CNRS, the Ville de Paris emergence program (2020 DAE 78), FRM amorçage (AJE201905008718), ATIP-Avenir starting grant R21045DS and the Laboratoire d'Excellence (Labex) DEEP (ANR-11-LBX-0044, ANR-10-IDEX- 0001-02 PSL), ECOS-ANID C22S01-220029. R.E. was supported by the Springboard postdoctoral fellowship from Institut Curie and Labex DEEP.

Authors contribution

Conceptualization: R.E. and P.P.H.; Methodology and data collection: R.E., A.M., K.C., Y.S., P.D. and G.G.; Writing - Original Draft: R.E.; Writing - Review & Editing: R.E. and P.P.H.; Funding Acquisition: P.P.H.

Conflict of Interest

The authors declare no competing interests.

References

1. Bertrand, J.Y., Chi, N.C., Santoso, B., Teng, S., Stainier, D.Y.R., and Traver, D. (2010). Haematopoietic stem cells derive directly from aortic endothelium during development. Nature *464*, 108–111. 10.1038/nature08738.

2. Boisset, J.-C., van Cappellen, W., Andrieu-Soler, C., Galjart, N., Dzierzak, E., and Robin, C. (2010). In vivo imaging of haematopoietic cells emerging from the mouse aortic endothelium. Nature *464*, 116–120. 10.1038/nature08764.

3. Kissa, K., and Herbomel, P. (2010). Blood stem cells emerge from aortic endothelium by a novel type of cell transition. Nature *464*, 112–115. 10.1038/nature08761.

4. Elsaid, R., Soares-da-Silva, F., Peixoto, M., Amiri, D., Mackowski, N., Pereira, P., Bandeira, A., and Cumano, A. (2020). Hematopoiesis: A Layered Organization Across Chordate Species. Front. Cell Dev. Biol. *8*, 606642. 10.3389/fcell.2020.606642.

5. Herbomel, P., Thisse, B., and Thisse, C. (2001). Zebrafish Early Macrophages Colonize Cephalic Mesenchyme and Developing Brain, Retina, and Epidermis through a M-CSF Receptor-Dependent Invasive Process. Developmental Biology *238*, 274–288. 10.1006/dbio.2001.0393.

485 6. Bertrand, J.Y., Kim, A.D., Violette, E.P., Stachura, D.L., Cisson, J.L., and Traver, D. (2007).
486 Definitive hematopoiesis initiates through a committed erythromyeloid progenitor in
487 the zebrafish embryo. Development *134*, 4147–4156. 10.1242/dev.012385.

488 7. Ferrero, G., Mahony, C.B., Dupuis, E., Yvernogeau, L., Di Ruggiero, E., Miserocchi, M.,
489 Caron, M., Robin, C., Traver, D., Bertrand, J.Y., et al. (2018). Embryonic Microglia Derive
490 from Primitive Macrophages and Are Replaced by cmyb-Dependent Definitive Microglia
491 in Zebrafish. Cell Reports *24*, 130–141. 10.1016/j.celrep.2018.05.066.

492 8. Tian, Y., Xu, J., Feng, S., He, S., Zhao, S., Zhu, L., Jin, W., Dai, Y., Luo, L., Qu, J.Y., et al.
493 (2017). The first wave of T lymphopoiesis in zebrafish arises from aorta endothelium
494 independent of hematopoietic stem cells. Journal of Experimental Medicine *214*, 3347–
495 3360. 10.1084/jem.20170488.

496 9. Murayama, E., Kissa, K., Zapata, A., Mordelet, E., Briolat, V., Lin, H.-F., Handin, R.I., and
497 Herbomel, P. (2006). Tracing hematopoietic precursor migration to successive
498 hematopoietic organs during zebrafish development. Immunity *25*, 963–975.
499 10.1016/j.immuni.2006.10.015.

500 10. Ulloa, B.A., Habbsa, S.S., Potts, K.S., Lewis, A., McKinstry, M., Payne, S.G., Flores, J.C.,
501 Nizhnik, A., Feliz Norberto, M., Mosimann, C., et al. (2021). Definitive hematopoietic
502 stem cells minimally contribute to embryonic hematopoiesis. Cell Reports *36*, 109703.
503 10.1016/j.celrep.2021.109703.

504 11. Patel, S.H., Christodoulou, C., Weinreb, C., Yu, Q., da Rocha, E.L., Pepe-Mooney, B.J.,
505 Bowling, S., Li, L., Osorio, F.G., Daley, G.Q., et al. (2022). Lifelong multilineage
506 contribution by embryonic-born blood progenitors. Nature *606*, 747–753.
507 10.1038/s41586-022-04804-z.

508 12. Stachura, D.L., and Traver, D. (2011). Chapter 4 - Cellular Dissection of Zebrafish
509 Hematopoiesis. In Methods in Cell Biology The Zebrafish: Cellular and Developmental
510 Biology, Part B., H. W. Detrich, M. Westerfield, and L. I. Zon, eds. (Academic Press), pp.
511 75–110. 10.1016/B978-0-12-387036-0.00004-9.

512 13. Xu, J., Zhu, L., He, S., Wu, Y., Jin, W., Yu, T., Qu, J.Y., and Wen, Z. (2015). Temporal-
513 Spatial Resolution Fate Mapping Reveals Distinct Origins for Embryonic and Adult
514 Microglia in Zebrafish. Developmental Cell *34*, 632–641. 10.1016/j.devcel.2015.08.018.

515 14. McGrath, K.E., Frame, J.M., and Palis, J. (2015). Early hematopoiesis and macrophage
516 development. Semin Immunol *27*, 379–387. 10.1016/j.smim.2016.03.013.

517 15. Kissa, K., and Herbomel, P. (2010). Blood stem cells emerge from aortic endothelium by
518 a novel type of cell transition. Nature *464*, 112–115. 10.1038/nature08761.

519 16. Henninger, J., Santoso, B., Hans, S., Durand, E., Moore, J., Mosimann, C., Brand, M.,
520 Traver, D., and Zon, L. (2017). Clonal fate mapping quantifies the number of
521 haematopoietic stem cells that arise during development. Nat Cell Biol *19*, 17–27.
522 10.1038/ncb3444.

523 17. Herbomel, P., Thisse, B., and Thisse, C. (1999). Ontogeny and behaviour of early
524 macrophages in the zebrafish embryo. Development *126*, 3735–3745.
525 10.1242/dev.126.17.3735.

526 18. Ganis, J.J., Hsia, N., Trompouki, E., de Jong, J.L.O., DiBiase, A., Lambert, J.S., Jia, Z., Sabo,
527 P.J., Weaver, M., Sandstrom, R., et al. (2012). Zebrafish globin Switching Occurs in Two
528 Developmental Stages and is Controlled by the LCR. Dev Biol *366*, 185–194.
529 10.1016/j.ydbio.2012.03.021.

530 19. Sánchez-Iranzo, H., Galardi-Castilla, M., Sanz-Morejón, A., González-Rosa, J.M., Costa, R.,
531 Ernst, A., Sainz de Aja, J., Langa, X., and Mercader, N. (2018). Transient fibrosis resolves
532 via fibroblast inactivation in the regenerating zebrafish heart. Proc. Natl. Acad. Sci.
533 U.S.A. *115*, 4188–4193. 10.1073/pnas.1716713115.

534 20. Carney, T.J., and Mosimann, C. (2018). Switch and Trace: Recombinase Genetics in
535 Zebrafish. Trends Genet *34*, 362–378. 10.1016/j.tig.2018.01.004.

536 21. Langenau, D.M., Ferrando, A.A., Traver, D., Kutok, J.L., Hezel, J.-P.D., Kanki, J.P., Zon, L.I.,
537 Look, A.T., and Trede, N.S. (2004). In vivo tracking of T cell development, ablation, and
538 engraftment in transgenic zebrafish. Proc Natl Acad Sci U S A *101*, 7369–7374.
539 10.1073/pnas.0402248101.

540 22. Li, L., Yan, B., Shi, Y.-Q., Zhang, W.-Q., and Wen, Z.-L. (2012). Live Imaging Reveals
541 Differing Roles of Macrophages and Neutrophils during Zebrafish Tail Fin Regeneration. J
542 Biol Chem *287*, 25353–25360. 10.1074/jbc.M112.349126.

543 23. Elsaid, R., Meunier, S., Burlen-Defranoux, O., Soares-da-Silva, F., Perchet, T., Iturri, L.,
544 Freyer, L., Vieira, P., Pereira, P., Golub, R., et al. (2021). A wave of bipotent T/ILC-
545 restricted progenitors shapes the embryonic thymus microenvironment in a time-
546 dependent manner. Blood *137*, 1024–1036. 10.1182/blood.2020006779.

547 24. Soares-da-Silva, F., Freyer, L., Elsaid, R., Burlen-Defranoux, O., Iturri, L., Sismeiro, O.,
548 Pinto-do-Ó, P., Gomez-Perdiguero, E., and Cumano, A. (2021). Yolk sac, but not
549 hematopoietic stem cell-derived progenitors, sustain erythropoiesis throughout murine
550 embryonic life. J Exp Med *218*, e20201729. 10.1084/jem.20201729.

551 25. Palis, J. (2014). Primitive and definitive erythropoiesis in mammals. Frontiers in
552 Physiology *5*.

553 26. Lin, X., Zhou, Q., Zhao, C., Lin, G., Xu, J., and Wen, Z. (2019). An Ectoderm-Derived
554 Myeloid-like Cell Population Functions as Antigen Transporters for Langerhans Cells in
555 Zebrafish Epidermis. Developmental Cell *49*, 605-617.e5. 10.1016/j.devcel.2019.03.028.

556 27. Ellett, F., Pase, L., Hayman, J.W., Andrianopoulos, A., and Lieschke, G.J. (2011). mpeg1
557 promoter transgenes direct macrophage-lineage expression in zebrafish. Blood *117*,
558 e49–e56. 10.1182/blood-2010-10-314120.

559 28. Wynn, T.A., and Vannella, K.M. (2016). Macrophages in Tissue Repair, Regeneration, and
560 Fibrosis. Immunity *44*, 450–462. 10.1016/j.immuni.2016.02.015.

561 29. Morales, R.A., and Allende, M.L. (2019). Peripheral Macrophages Promote Tissue
562 Regeneration in Zebrafish by Fine-Tuning the Inflammatory Response. Front. Immunol.
563 *10*, 253. 10.3389/fimmu.2019.00253.

564 30. Nguyen-Chi, M., Laplace-Builhé, B., Travnickova, J., Luz-Crawford, P., Tejedor, G.,
565 Lutfalla, G., Kissa, K., Jorgensen, C., and Djouad, F. (2017). TNF signaling and
566 macrophages govern fin regeneration in zebrafish larvae. Cell Death Dis *8*, e2979–
567 e2979. 10.1038/cddis.2017.374.

568 31. Petrie, T.A., Strand, N.S., Tsung-Yang, C., Rabinowitz, J.S., and Moon, R.T. (2014).
569 Macrophages modulate adult zebrafish tail fin regeneration. Development *141*, 2581–
570 2591. 10.1242/dev.098459.

571 32. Curado, S., Stainier, D.Y.R., and Anderson, R.M. (2008). Nitroreductase-mediated
572 cell/tissue ablation in zebrafish: a spatially and temporally controlled ablation method
573 with applications in developmental and regeneration studies. Nat Protoc *3*, 948–954.
574 10.1038/nprot.2008.58.

575 33. Soza-Ried, C., Hess, I., Netuschil, N., Schorpp, M., and Boehm, T. (2010). Essential role of
576 *c-myb* in definitive hematopoiesis is evolutionarily conserved. Proc. Natl. Acad. Sci.
577 U.S.A. *107*, 17304–17308. 10.1073/pnas.1004640107.

578 34. He, S., Chen, J., Jiang, Y., Wu, Y., Zhu, L., Jin, W., Zhao, C., Yu, T., Wang, T., Wu, S., et al.
579 (2018). Adult zebrafish Langerhans cells arise from hematopoietic stem/progenitor cells.
580 eLife *7*, e36131. 10.7554/eLife.36131.

581 35. Travnickova, J., Tran Chau, V., Julien, E., Mateos-Langerak, J., Gonzalez, C., Lelièvre, E.,
582 Lutfalla, G., Tavian, M., and Kissa, K. (2015). Primitive macrophages control HSPC
583 mobilization and definitive haematopoiesis. Nat Commun *6*, 6227.
584 10.1038/ncomms7227.

585 36. Gomez Perdiguero, E., Klapproth, K., Schulz, C., Busch, K., Azzoni, E., Crozet, L., Garner,
586 H., Trouillet, C., de Bruijn, M.F., Geissmann, F., et al. (2015). Tissue-resident
587 macrophages originate from yolk-sac-derived erythro-myeloid progenitors. Nature *518*,
588 547–551. 10.1038/nature13989.

589 37. Yokomizo, T., Ideue, T., Morino-Koga, S., Tham, C.Y., Sato, T., Takeda, N., Kubota, Y.,
590 Kurokawa, M., Komatsu, N., Ogawa, M., et al. (2022). Independent origins of fetal liver
591 haematopoietic stem and progenitor cells. Nature *609*, 779–784. 10.1038/s41586-022-
592 05203-0.

593 38. Fanti, A.-K., Busch, K., Greco, A., Wang, X., Cirovic, B., Shang, F., Nizharadze, T., Frank, L.,
594 Barile, M., Feyerabend, T.B., et al. (2023). Flt3- and Tie2-Cre tracing identifies
595 regeneration in sepsis from multipotent progenitors but not hematopoietic stem cells.
596 Cell Stem Cell *0*. 10.1016/j.stem.2022.12.014.

597 39. Jagadeeswaran, P., Lin, S., Weinstein, B., Hutson, A., and Kim, S. (2010). Loss of GATA1
598 and gain of FLI1 expression during thrombocyte maturation. Blood Cells, Molecules, and
599 Diseases *44*, 175–180. 10.1016/j.bcmd.2009.12.012.

600 40. Hsia, N., and Zon, L.I. (2005). Transcriptional regulation of hematopoietic stem cell
601 development in zebrafish. Experimental Hematology *33*, 1007–1014.
602 10.1016/j.exphem.2005.06.013.

603 41. Renaud, O., Herbomel, P., and Kissa, K. (2011). Studying cell behavior in whole zebrafish
604 embryos by confocal live imaging: application to hematopoietic stem cells. Nat Protoc *6*,
605 1897–1904. 10.1038/nprot.2011.408.

606 42. Schindelin, J., Arganda-Carreras, I., Frise, E., Kaynig, V., Longair, M., Pietzsch, T.,
607 Preibisch, S., Rueden, C., Saalfeld, S., Schmid, B., et al. (2012). Fiji: an open-source
608 platform for biological-image analysis. Nat Methods *9*, 676–682. 10.1038/nmeth.2019.

609 43. Pei, W., Tanaka, K., Huang, S.C., Xu, L., Liu, B., Sinclair, J., Idol, J., Varshney, G.K., Huang,
610 H., Lin, S., et al. (2016). Extracellular HSP60 triggers tissue regeneration and wound
611 healing by regulating inflammation and cell proliferation. npj Regen Med *1*, 1–11.
612 10.1038/npjregenmed.2016.13.

613

Graphical abstract

Steady state

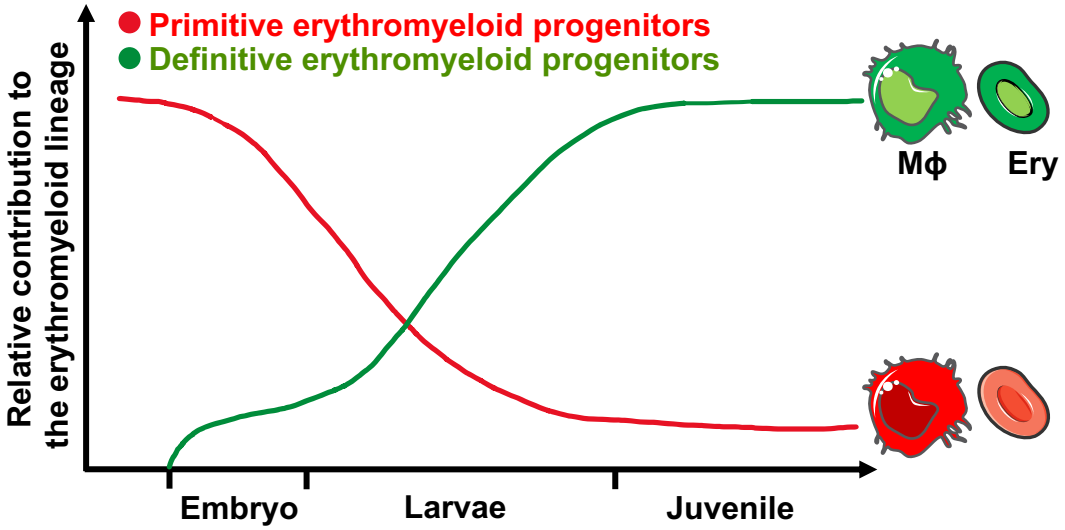

Caudal fin Injury

During embryonic stages:

During early larval developmental stages:

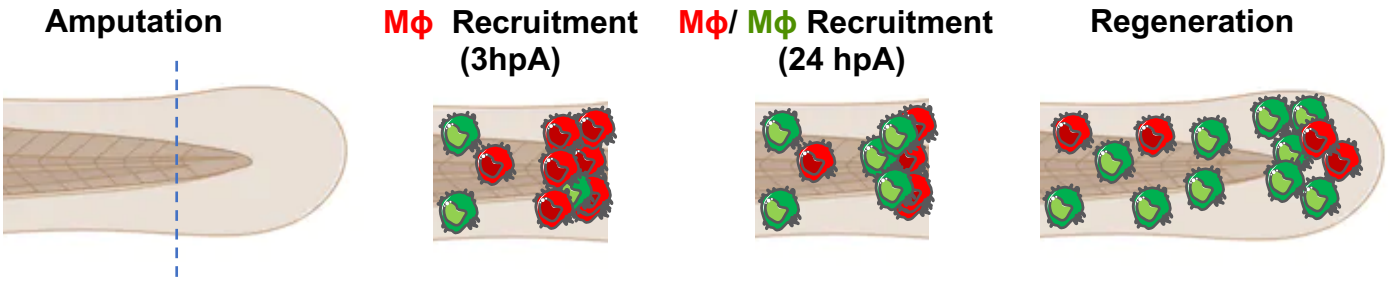

During early larval developmental stages upon ablation of definitive macrophages:

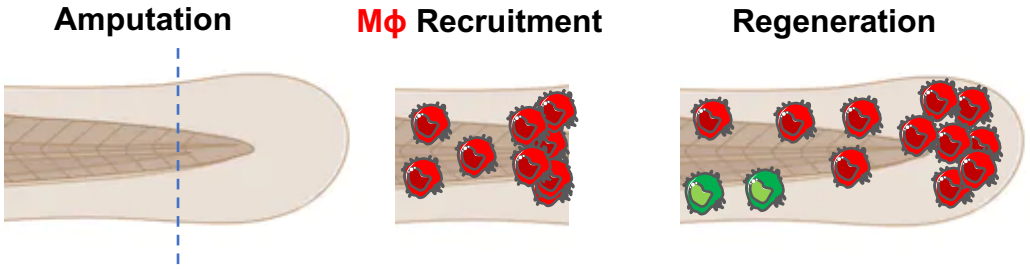

Figure 1

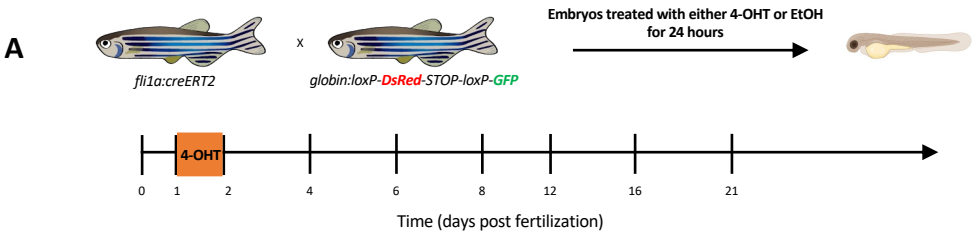
A
fli1a:creERT2
x
globin:loxP-DsRed-STOP-loxP-GFP
Embryos treated with either 4-OHT or EtOH for 24 hours
4-OHT
0
1
2
4
6
8
12
16
21
Time (days post fertilization)

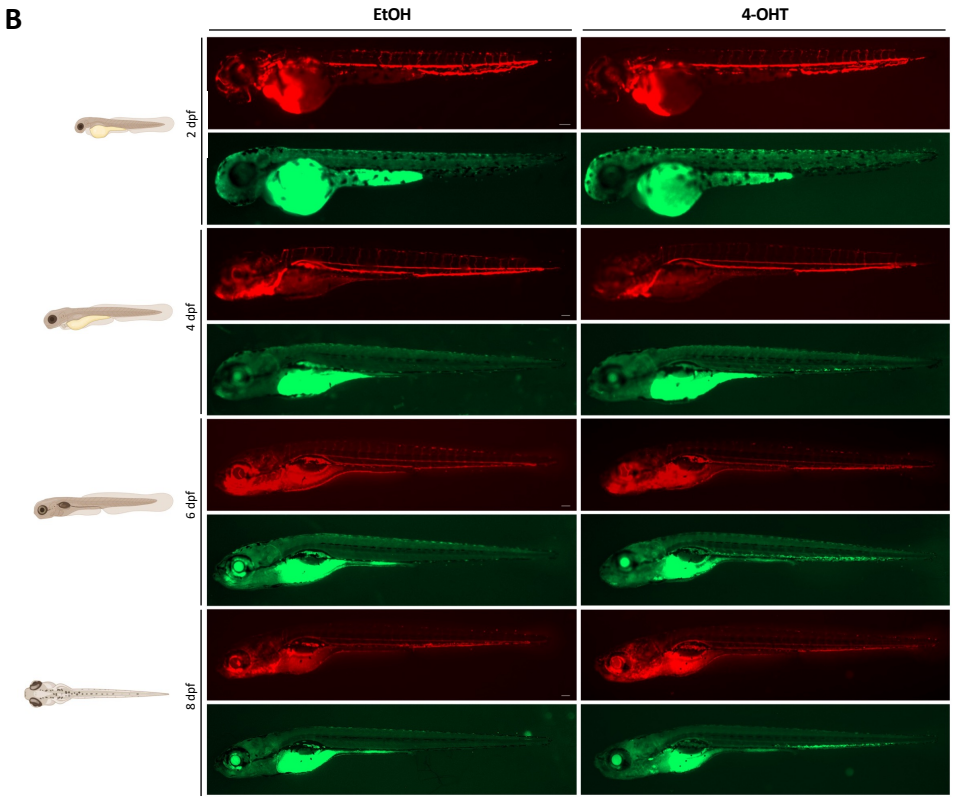
B
EtOH
4-OHT
2 dpf
4 dpf
6 dpf
8 dpf

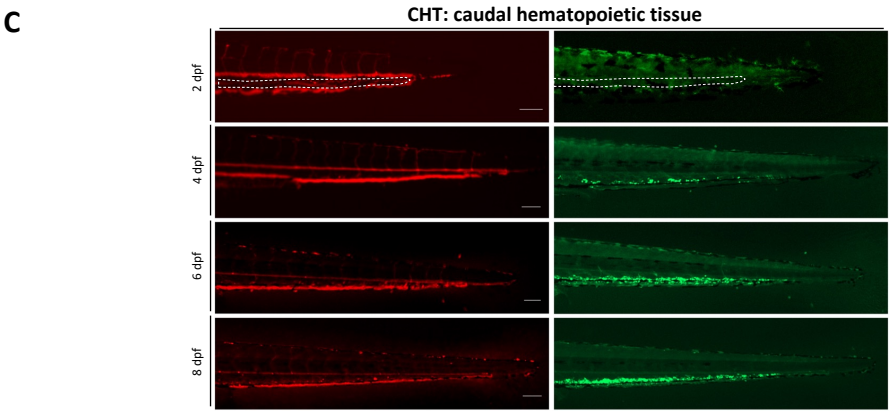
C
CHT: caudal hematopoietic tissue
2 dpf
4 dpf
6 dpf
8 dpf

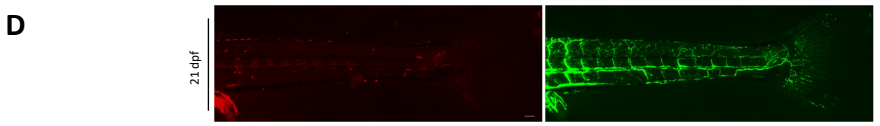
D
21 dpf

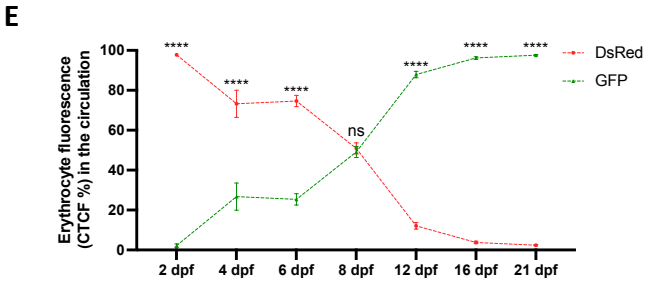
E
Erythrocyte fluorescence (CTCF %) in the circulation
100
80
60
40
20
0
****
ns
2 dpf
4 dpf
6 dpf
8 dpf
12 dpf
16 dpf
21 dpf
DsRed
GFP

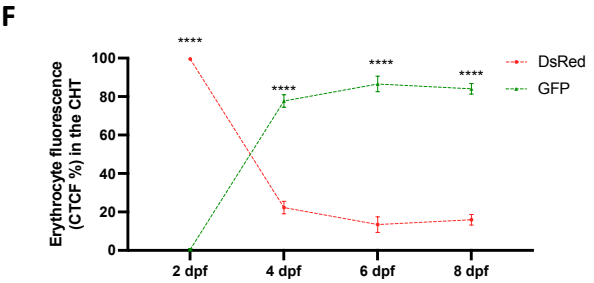
F
Erythrocyte fluorescence (CTCF %) in the CHT
100
80
60
40
20
0
****
2 dpf
4 dpf
6 dpf
8 dpf
DsRed
GFP

Figure 2

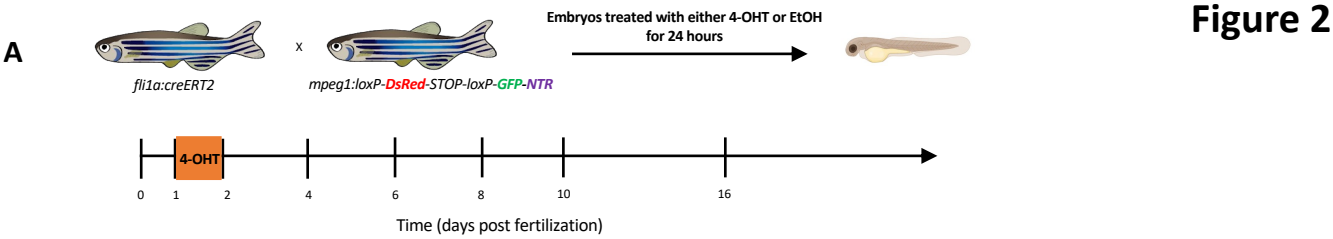
A
fli1a:creERT2
x
mpeg1:loxP-DsRed-STOP-loxP-GFP-NTR
Embryos treated with either 4-OHT or EtOH for 24 hours
4-OHT
0
1
2
4
6
8
10
16
Time (days post fertilization)

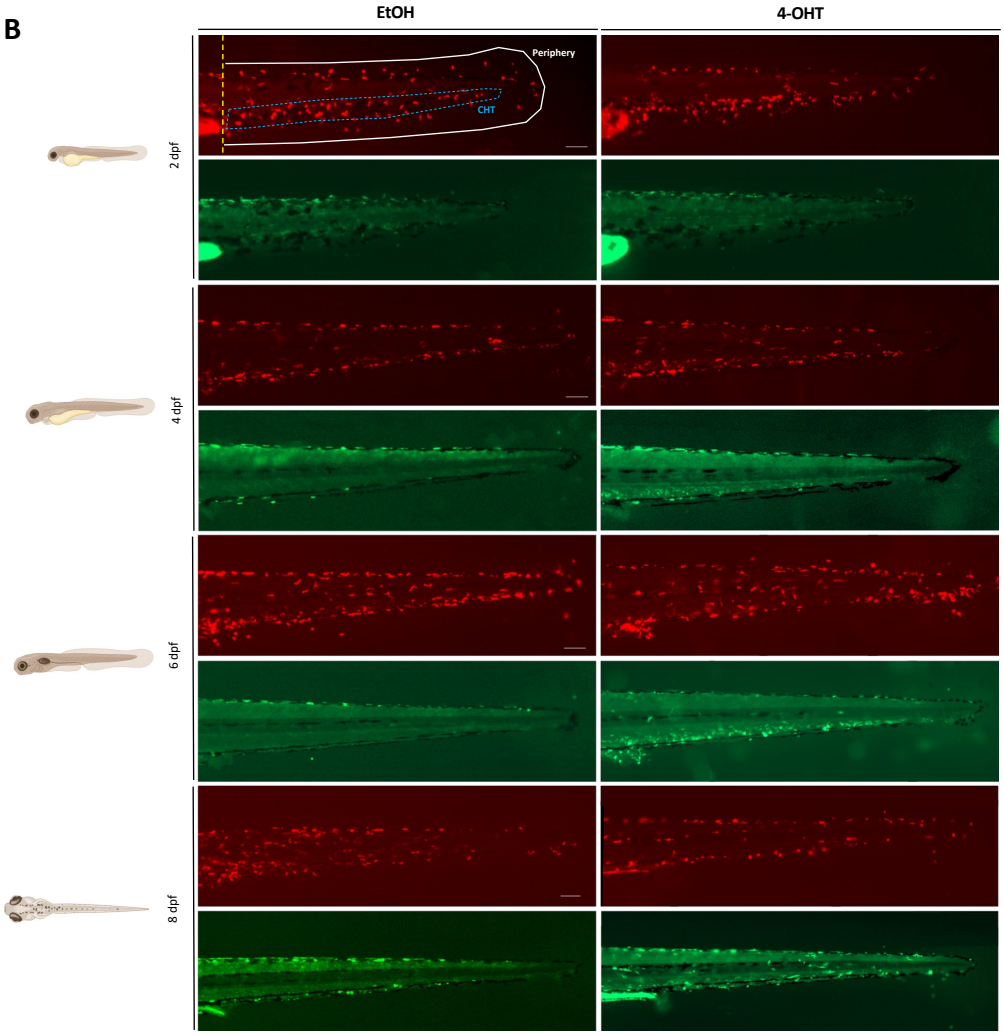
B
EtOH
4-OHT
Periphery
CHT
2 dpf
4 dpf
6 dpf
8 dpf

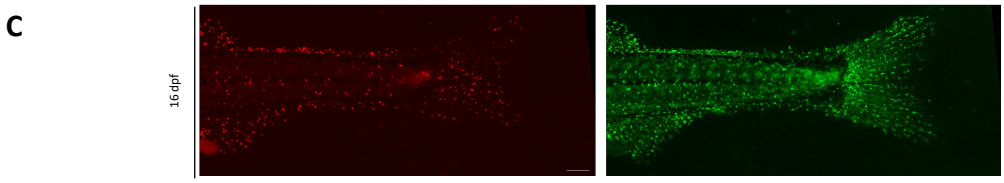
C
16 dpf

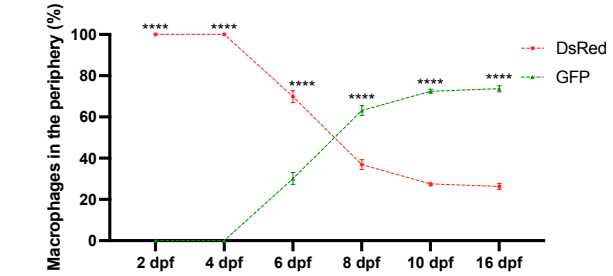
D
Macrophages in the periphery (%)
100
80
60
40
20
0
2 dpf
4 dpf
6 dpf
8 dpf
10 dpf
16 dpf
****
DsRed
GFP

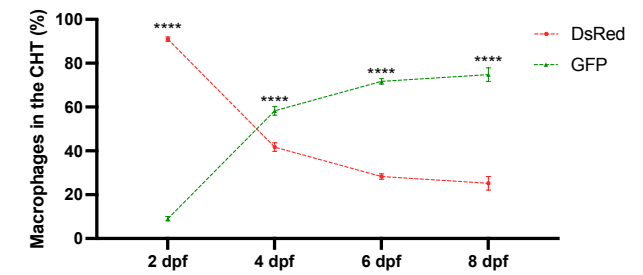
E
Macrophages in the CHT (%)
100
80
60
40
20
0
2 dpf
4 dpf
6 dpf
8 dpf
****
DsRed
GFP

Figure 3

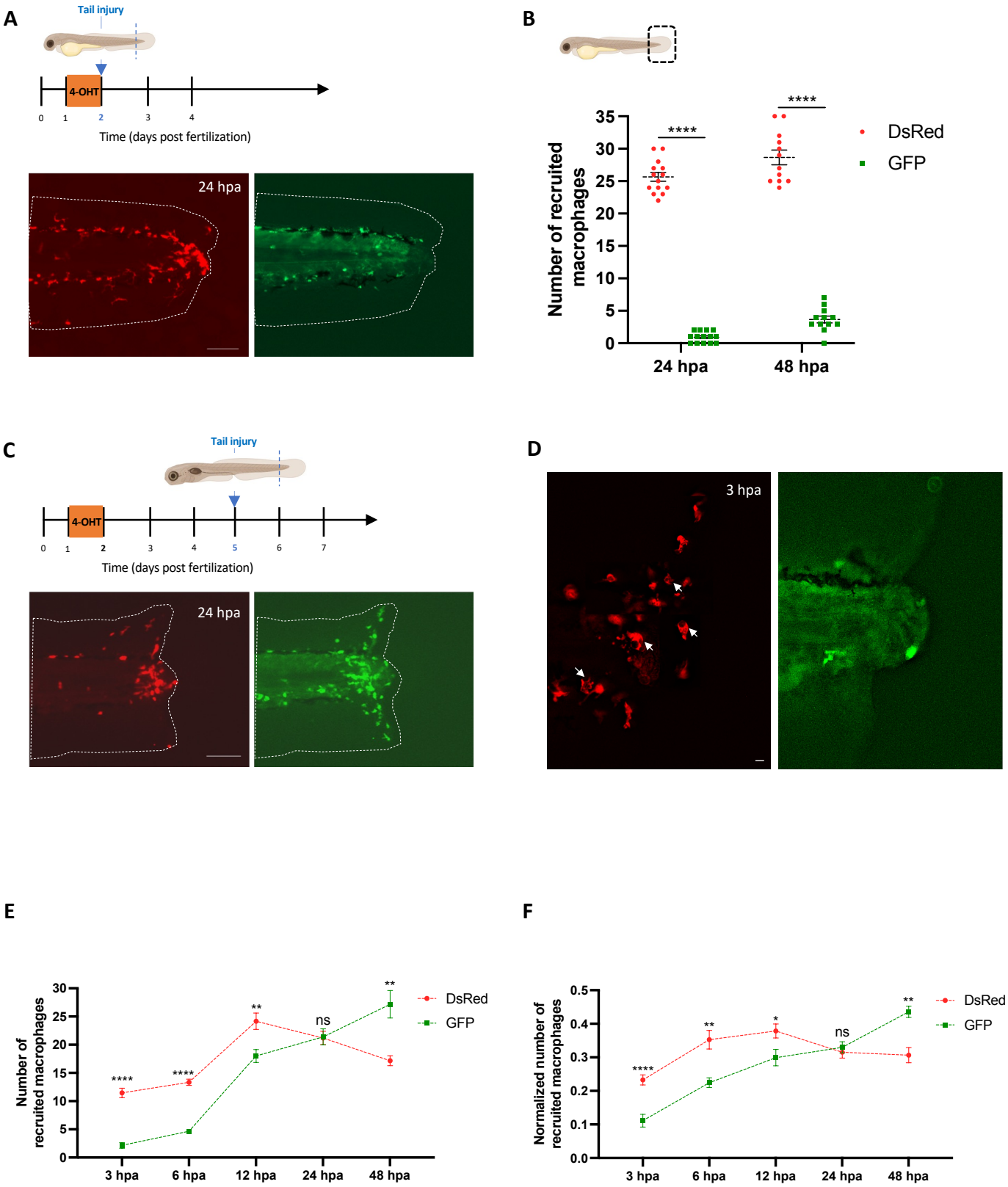
A
Tail injury
4-OHT
0
1
2
3
4
Time (days post fertilization)
24 hpa
B
Number of recruited macrophages
35
30
25
20
15
10
5
0
****
****
24 hpa
48 hpa
DsRed
GFP
C
Tail injury
4-OHT
0
1
2
3
4
5
6
7
Time (days post fertilization)
24 hpa
D
3 hpa
E
Number of recruited macrophages
30
25
20
15
10
5
0
****
****
**
ns
**
3 hpa
6 hpa
12 hpa
24 hpa
48 hpa
DsRed
GFP
F
Normalized number of recruited macrophages
0.5
0.4
0.3
0.2
0.1
0.0
****
**
*
ns
**
3 hpa
6 hpa
12 hpa
24 hpa
48 hpa
DsRed
GFP

Figure 4

A

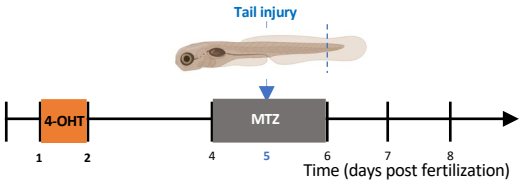

B

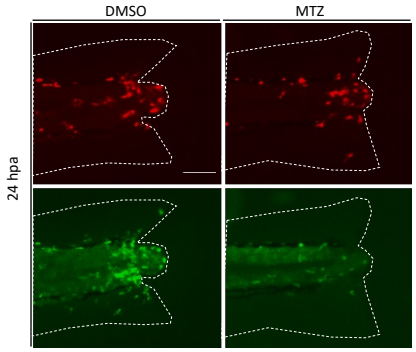

C

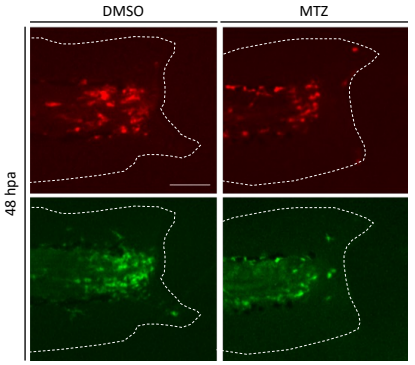

D

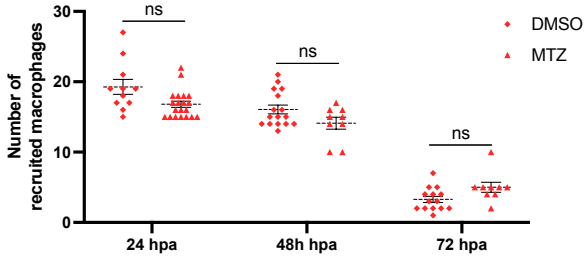

E

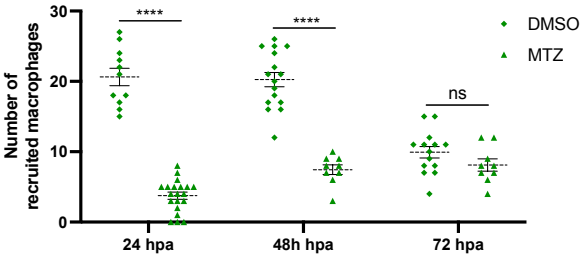

F

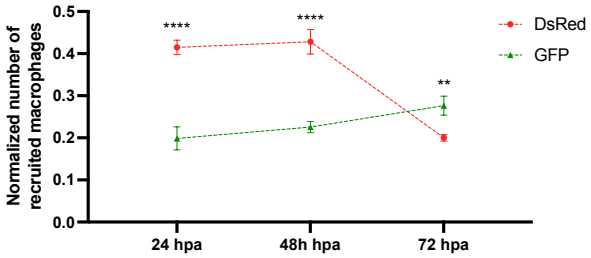

G

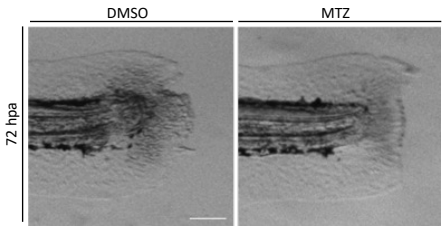

H

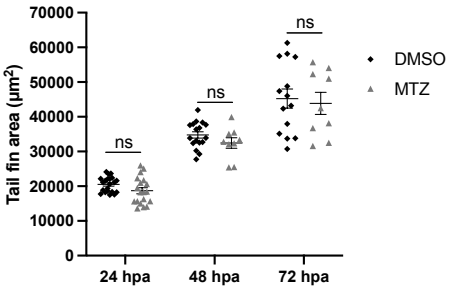

I

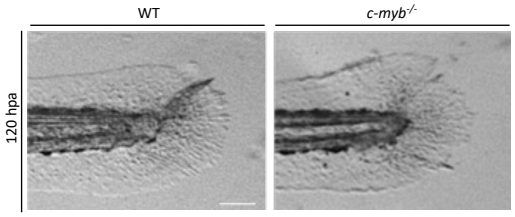

J

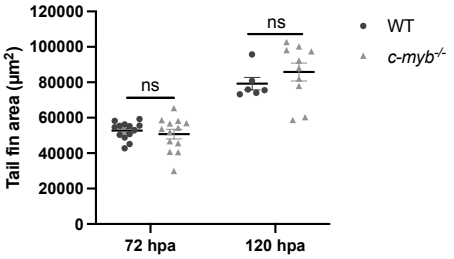

Figure 5

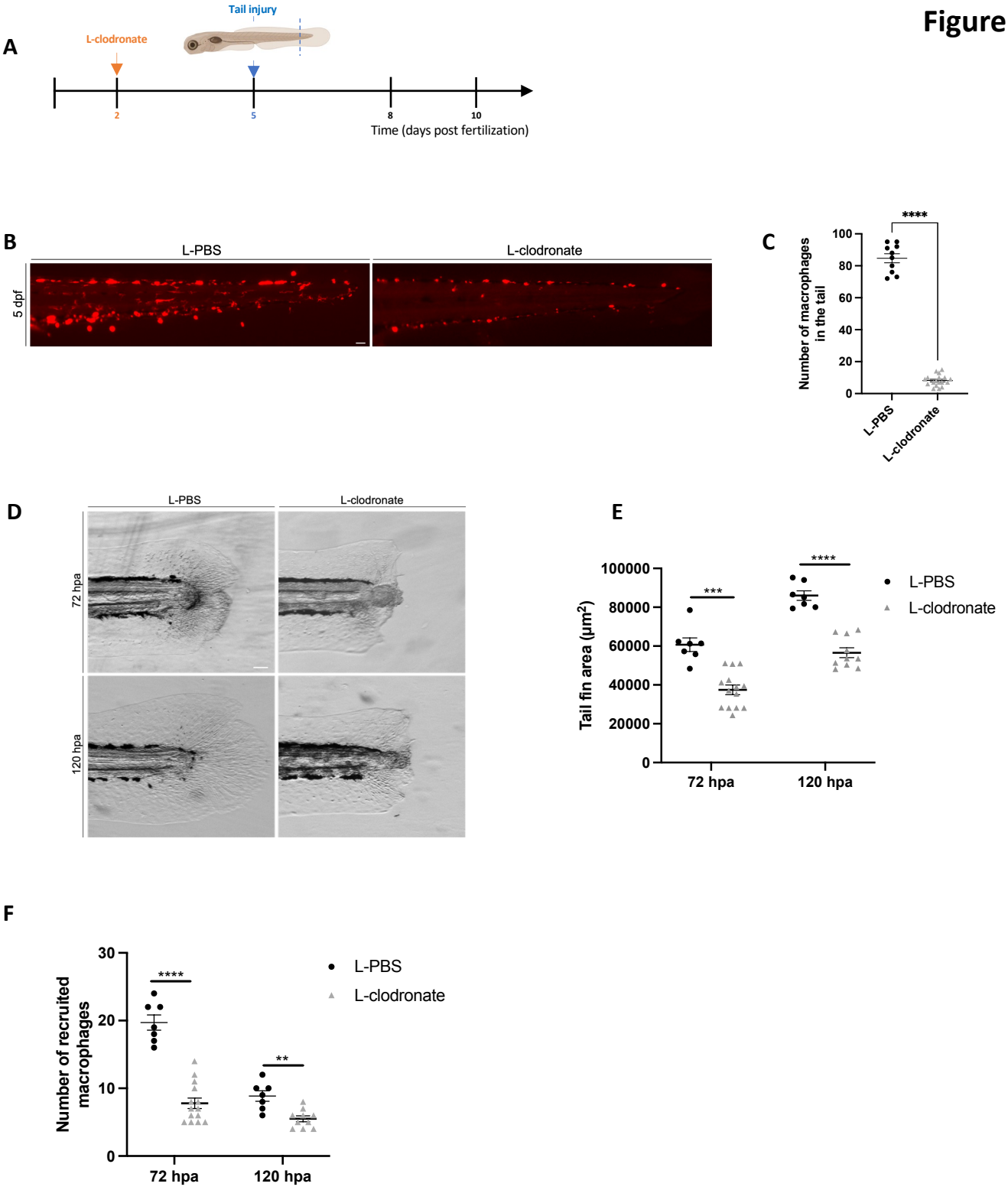
A
L-clodronate
Tail injury
2
5
8
10
Time (days post fertilization)
B
L-PBS
L-clodronate
5 dpf
C
Number of macrophages in the tail
****
L-PBS
L-clodronate
D
L-PBS
L-clodronate
72 hpa
120 hpa
E
Tail fin area (µm²)
***
****
L-PBS
L-clodronate
72 hpa
120 hpa
F
Number of recruited macrophages
****
**
L-PBS
L-clodronate
72 hpa
120 hpa

Supp Figure 1

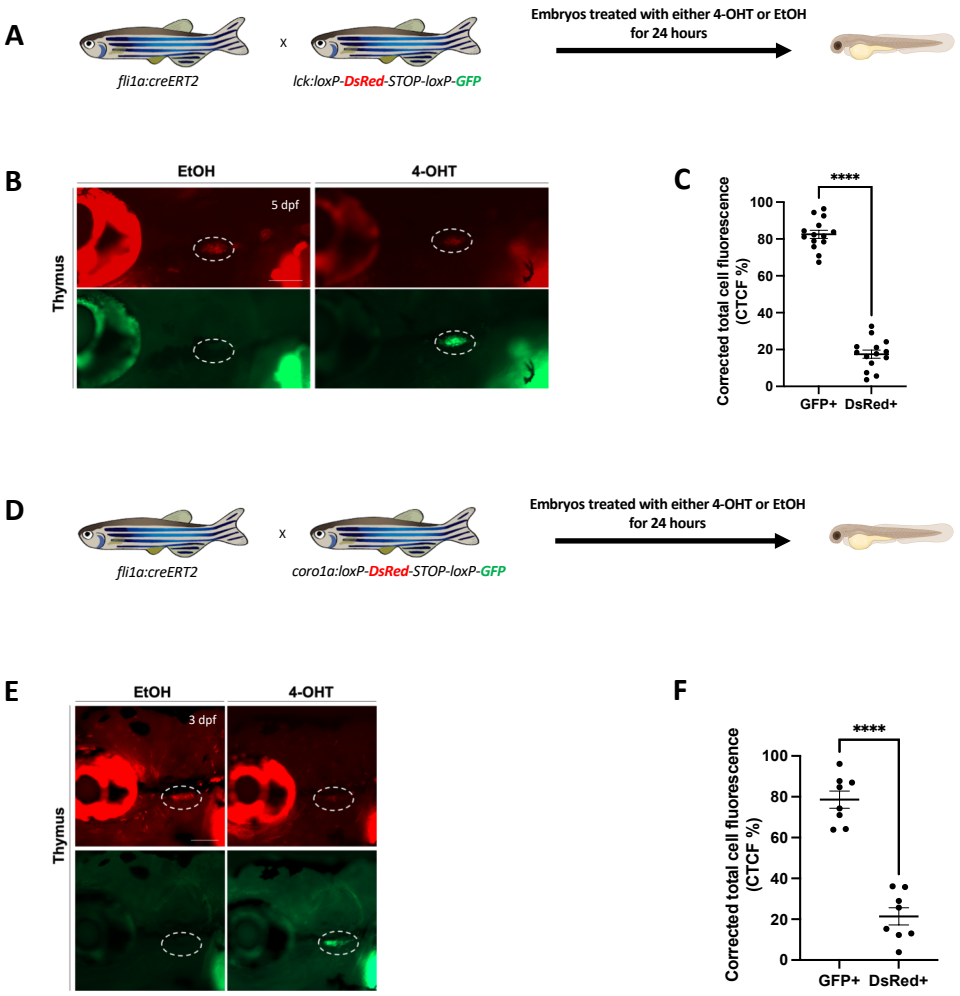

CHT: caudal hematopoietic tissue

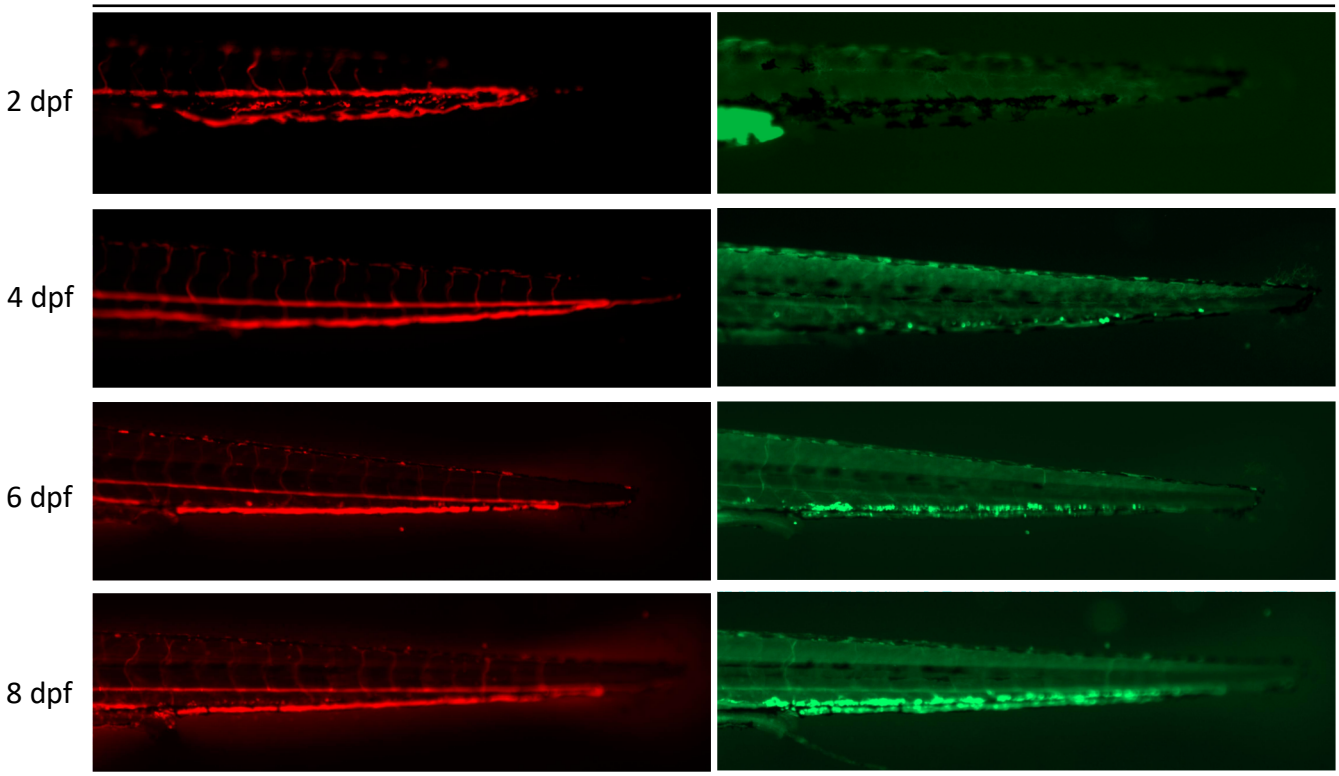

Supp Figure 2.Related to Fig. 2

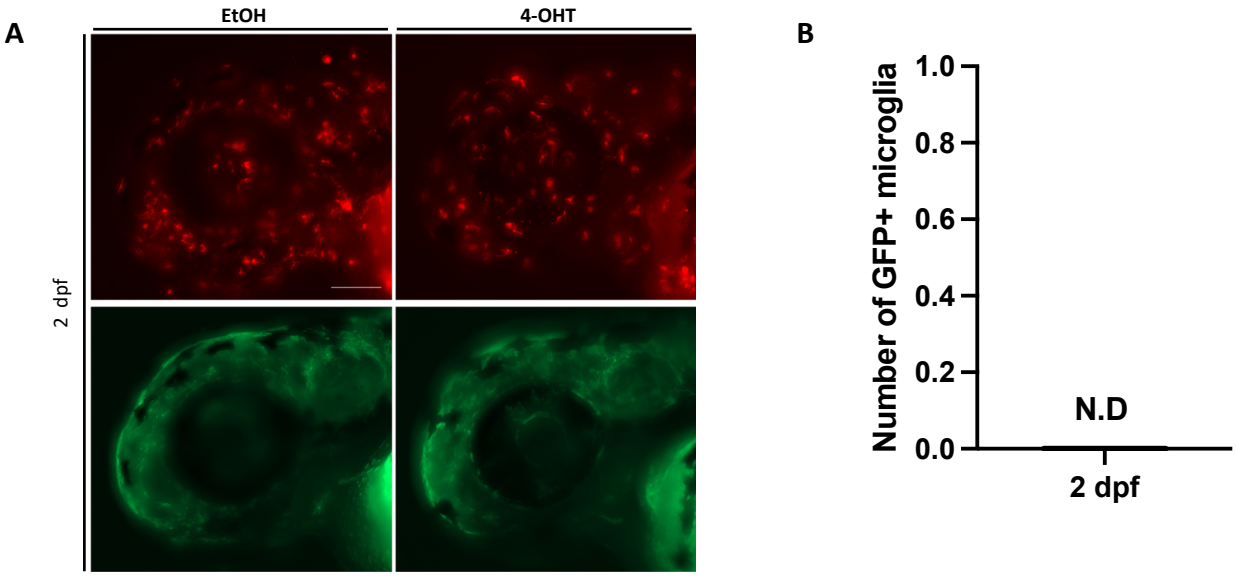

Supp Figure 3. Related to Fig. 3 and 4

A

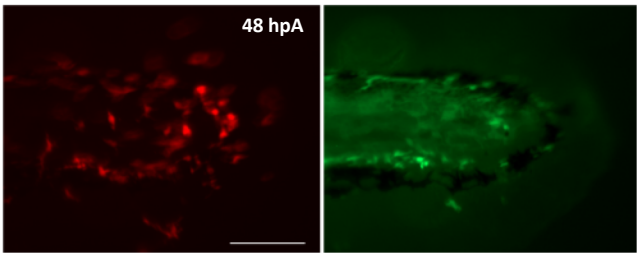

B

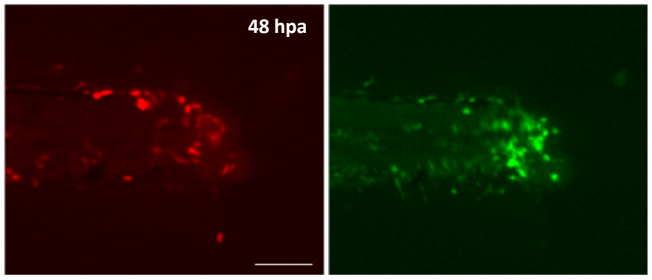

C

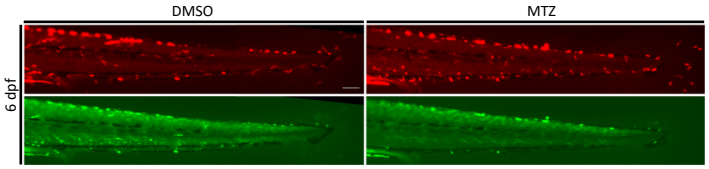

D

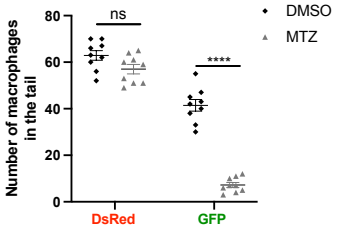

E

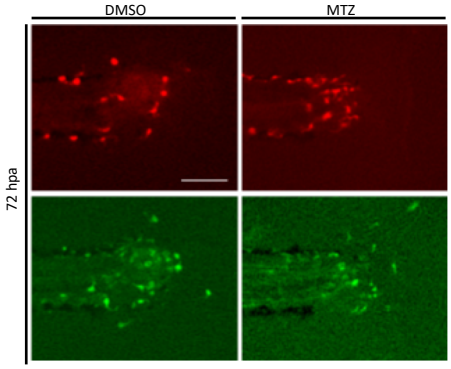

F

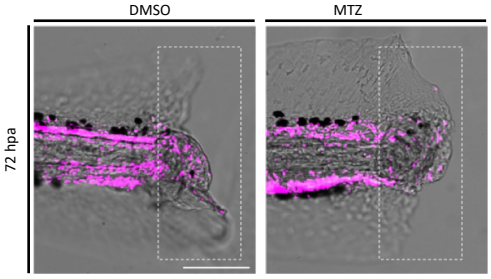

G

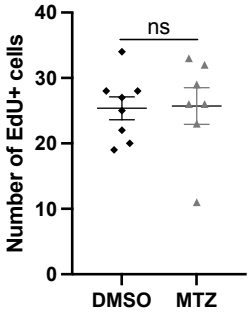

Figure 1: Tracing the contribution of definitive hematopoietic waves to the erythroid lineage in the embryoand early larvae

(A) Scheme of the 4-OHT-inducible transgenic lines used to assess the contribution of definitive hematopoietic waves to the erythroid lineage.
(B) Fluorescent images of EtOH non-switched controls (left) and 4-OHT-induced (right) *Tg(fli1a:creERT2;globin:Switch)* embryos and larvae (2 dpf-8 dpf). Scale bars, 100 µm. Quantification of erythrocytes in circulation are shown in (E).
(C) Fluorescent images of 4-OHT-induced *Tg(fli1a:creERT2;globin:Switch)* embryos and larvae (2-8 dpf) in the CHT region. Non-switched primitive erythrocytes (left) and definitive erythrocytes (right). Scale bars, 100 µm. quantification of erythrocytes in the CHT are shown in (F).
(D) Fluorescent images of 4-OHT-induced *Tg(fli1a:creERT2;globin:Switch)* (21 dpf) in the circulation. Scale bar,100 µm. Non-switched primitive erythrocytes (left) and definitive erythrocytes (right). Quantification of erythrocytes in the circulation are shown in (E).
(E) Quantification of DsRed and GFP fluorescence intensity percentage in the circulation over a time course of 2-21 dpf. (2 dpf n=6; 4 dpf n=4; 6 dpf n=5; 8 dpf n=4; 12 dpf; 16 dpf n=6 and 21 dpf n=5). Mean ± SEM of the $DsRed^+$ and GFP^+ corrected total cell fluorescence (CTCF) percentage at each time point is shown. Two-way ANOVA with Sidak's multiple comparison was used for this analysis. $^{****}p \leq 0.0001$.
(F) Quantification of DsRed and GFP fluorescence intensity percentage in the CHT over a time course of 2-8 dpf. (2 dpf n=6; 4 dpf n=4; 6 dpf n=5 and 8 dpf n=4). Mean ± SEM of the $DsRed^+$ and GFP^+ corrected total cell fluorescence (CTCF) percentage at each time point is shown. Two-way ANOVA with Sidak's multiple comparison was used for this analysis. $^{****}p \leq 0.0001$.

Figure 2: Tracing the contribution of definitive hematopoietic waves to macrophages in the embryo and early larvae

(A) Scheme of the 4-OHT-inducible transgenic lines used to assess the contribution of definitive hematopoietic waves to the macrophage lineage.
(B) Fluorescent images of EtOH non-switched controls (left) and 4-OHT-induced (right) *Tg(fli1a:creERT2;mpeg1:Switch)* embryos and larvae (2-8 dpf). Macrophages were considered as peripheral macrophages (white area) or CHT-resident macrophages (blue area). Scale bars, 100 µm. Quantification of macrophages in the periphery and the CHT are shown in (D) and (E) respectively.
(C) Fluorescent images of 4-OHT-induced *Tg(fli1a:creERT2;mpeg1:Switch)* (16 dpf) in the periphery. Scale bar, 500 µm. Non-switched primitive macrophages (left) and definitive macrophages (right). Quantification of macrophages in the periphery are shown in (D).
(D) Quantification of DsRed+ and GFP+ macrophages in the periphery over a time course of 2-16 dpf. (2 dpf n=6; 4 dpf n=11; 6 dpf n=7; 8 dpf n=4; 10 dpf n=5 and 16 dpf n=5). Mean ± SEM of the $DsRed^+$ and GFP^+ macrophage number at each time point is shown. Two-way ANOVA with Sidak's multiple comparison was used for this analysis. $^{****}p \leq 0.0001$.
(E) Quantification of DsRed+ and GFP+ macrophages in the CHT over a time course of 2-8dpf. (2 dpf n=6; 4 dpf n=11; 6 dpf n=7 and 8 dpf n=4). Mean ± SEM of the $DsRed^+$ and GFP^+ macrophage numberat each time point is shown. Two-way ANOVA with Sidak's multiple comparison was used for this analysis. $^{****}p \leq 0.0001$.

Figure 3: Ontogenetically distinct macrophages exhibit different migration behavior and recruitment aftertissue injury at early developmental stages

(A) Diagram showing the amputation plan, tail fin of *Tg(fli1a:creERT2;mpeg1:Switch)* were amputated at 2 dpf and macrophages recruitment to the site of injury was analyzed. Representative images are shown at 24 hpa.Scale bar: 100µm.
(B) Diagram showing the counting region in the larvae. Quantification of DsRed+ and GFP+ macrophages at the site of injury at 24 hpa (n=14) and 48 hpa (n=12). Mean ± SEM of the $DsRed^+$ and GFP^+ macrophage number at each time point is shown. $^{****}p \leq 0.0001$.

(C) Diagram showing the amputation plan, tail fin of *Tg(fli1a:creERT2;mpeg1:Switch)* were amputated at 5 dpf and macrophage numbers at the site of injury was analyzed. Representative images are shown at 24 hpa. Scale bar: 100µm.
(D) Tail fin of *Tg(fli1a:creERT2;mpeg1:Switch)* were amputated at 5 dpf and macrophage numbers at the site of injury was analyzed. Representative images are shown at 3 hpa. White arrows indicate the primitive macrophages with big vacuoles. Scale bar: 10µm.
(E) Quantification of DsRed+ and GFP+ macrophages at the site of injury at 3 hpa (n=13); 6 hpa (n=6); 12 hpa (n=6); 24 hpa (n=10) and 48 hpa (n=6). Mean ± SEM of the $DsRed^+$ and GFP^+ macrophage number at each time point is shown. ns, $p>0.05$; $^{**}p \leq 0.01$; $^{****}p \leq 0.0001$.
(F) Quantification of DsRed+ and GFP+ macrophages at the site of injury at 3 hpa (n=13); 6 hpa (n=6); 12 hpa (n=6); 24 hpa (n=10) and 48 hpa (n=6). Mean ± SEM of the $DsRed^+$ and GFP^+ macrophage numbers at each time point is shown. Quantification was normalized by the number of total macrophages in the tail of the respective larvae (the sum of peripheral, CHT and recruited macrophages of distinct origins). ns, $p>0.05$; $^{*}p \leq 0.05$; $^{**}p \leq 0.01$; $^{****}p \leq 0.0001$.

Figure 4: Selective ablation of definitive macrophages does not impair tail fin regeneration in early larvae

(A) Diagram showing the macrophage ablation and tail fin amputation strategy.
(B-C) Switched *Tg(fli1a:creERT2;mpeg1:Switch)* larvae were treated with DMSO as a control, or metronidazole (MTZ) to ablate definitive macrophages. Treatments were performed from 4 to 6 dpf and tail fins were amputated at 5 dpf. Representative images are shown 24 hpa in (B) and 48 hpa in (C). Scale bars: 100 µm.
(D) Quantification of DsRed+ macrophages in the tail region at 24, 48 and 72 hpa in larvae treated at 4 dpf with either DMSO or MTZ for 48 hours (24 hpa: DMSO=11, MTZ =20; 48 hpa: DMSO n=16, MTZ n=9; 72 hpa: DMSO n=14, MTZ n=9). Mean ± SEM ofthe $DsRed^+$ macrophage number is shown. ns, $p>0.05$.
(E) Quantification of GFP+ macrophages in the tail region at 24, 48 and 72 hpa in larvae treated at 4 dpf with either DMSO or MTZ for 48 hours (24 hpa: DMSO=11, MTZ =20; 48 hpa: DMSO n=16, MTZ n=9; 72 hpa: DMSO n=14, MTZ n=9). Mean ± SEM of the GFP^+ macrophages is shown. ns, $p>0.05$; $^{****}p \leq 0.0001$.
(F) Quantification of DsRed+ and GFP+ macrophages at the site of injury at 24, 48 and 72 hpa. Quantification was normalized bythe number of total macrophages in the tail of the respective larvae (the sum of peripheral, CHT and recruited macrophages of distinct origins). $^{**}p \leq 0.01$; $^{****}p \leq 0.0001$.
(G) Representative images of regenerating tail fins of larvae at 72 hpa. Larvae were treated with either DMSO or MTZ. Scale bars: 100 µm.
(H) Tail fin area quantification of regenerating tail fins at 24, 48 and 72 hpa in larvae treated with either DMSO or MTZ (24 hpa: DMSO n=21, MTZ n=20; 48 hpa: DMSO n=17, MTZ n=9; 72 hpa: DMSO n=14, MTZ n=9). Mean ± SEM of the tail fin area is shown. ns, $p>0.05$.
(I) Representative images of regenerating tail fins of *cmyb*^{null} and WT larvae at 120 hpa. Scale bars: 100 µm.
(J) Tail fin area quantification of regenerating tail fins of *cmyb*^{null} and WT larvae at 72 hpa and 120 hpa (72 hpa: *cmyb*^{null} n=13, WT n=13; 120 hpa: *cmyb*^{null} n=10, WT n=6). Mean ± SEM of the tail fin area is shown. ns, $p>0.05$.

Figure 5: Depletion of primitive macrophages impairs tail fin regeneration in early larvae

(A) Diagram showing the macrophage depletion using L-clodronate injection and tail fin amputation plan.
(B) *Tg(mpeg1:Switch)* larvae were injected at 48 hpf with L-PBS as a control, or L-clodronate (L-clo) to deplete primitive macrophages. Representative images are shown at 5 dpf. Scale bars: 100 µm.
(C) Quantification of DsRed+ macrophages in the tail region at 5 dpf in larvae injected with either L-PBS (n=10) or L-clo (n=18). Mean ± SEM of the $DsRed^+$ macrophages is shown. $^{****}p \leq 0.0001$.
(D) Representative images of regenerating tail fins of larvae at 72 and 120 hpa. Larvae were injected with either L-PBS or L-clodronate. Scale bars: 100 µm.
(E) Tail fin area quantification of regenerating tail fins at 72 and 120 hpa in larvae injected with either L-PBS or L-clodronate (72 hpa: L-PBS n=7, L-clo n=14; 72 hpa: L-PBS n=7, L-clo n=10). Mean ± SEM of the tail fin area is shown. $^{***}p \leq 0.001$; $^{****}p \leq 0.0001$.
(F) Representative images of macrophages at the site of injury at 72 and 120 hpa in larvae injected with either L-PBS or L-clodronate. Scale bars: 100 µm.
(G) Quantification of macrophages at the site of injury at 72 and 120 hpa (72 hpa: L-PBS=7, L-clo n=14; 120 hpa: L-PBS=7, L-clo n=10). Mean ± SEM of the macrophage number is shown. $^{**}p \leq 0.01$; $^{****}p \leq 0.0001$.

Sup. Fig. 1. Labeling strategy and the labeling efficiency of using thymocytes as a positive read out with *lck*:switch and *coro1a*:switch transgenic lines.

(A) Scheme of the 4-OHT-inducible *Tg(fli1a:creERT2;lck:Switch)* line used to assess the efficiency of the labelling strategy.

(B) Fluorescent images of EtOH non-switched controls (left) and 4-OHT-induced (right) *Tg(fli1a:creERT2;lck:Switch)* thymocytes at 5 dpf larvae. Representative images are shown. Scale bars, 100 µm.

(C) Quantification of DsRed and GFP fluorescence intensity percentage in the thymic region was measured at 5dpf (n=14). Mean ± SEM of the DsRed$^+$ and GFP$^+$ corrected total cell fluorescence (CTCF) percentage is shown. ****p≤ 0.0001

(D) Scheme of the 4-OHT-inducible *Tg(fli1a:creERT2; coro1a:Switch)* line used to assess the efficiency of the labelling strategy.

(E) Fluorescent images of EtOH non-switched controls (left) and 4-OHT-induced (right) *Tg(fli1a:creERT2;coro1a:Switch)* thymocytes at 3 dpf embryos. Representative images are shown. Scale bars, 100 µm.

(F) Quantification of DsRed and GFP fluorescence intensity percentage in the thymic region was measured at 3dpf (n=8). Mean ± SEM of the DsRed$^+$ and GFP$^+$ corrected total cell fluorescence (CTCF) percentage is shown. ****p≤ 0.0001

Supp videos related to Fig.1. Fluorescence imaging of 4-OHT-induced *Tg(fli1a:creERT2;globin:Switch)* embryos and larvae over a time course of 2- 8 dpf. Videos are assembled from different Z-stacks projections at each defined developmental stage.

Supp Fig.2. Quantification of GFP+ microglia in the head region at 2 dpf embryos. related to Fig.2

(A) Fluorescent images of EtOH non-switched controls (left) and 4-OHT-induced (right) *Tg(fli1a:creERT2;mpeg1:Switch)* head regions in the developing embryos at 2 dpf. Representative images are shown. Scale bar: 100µm.

(B) Quantification of GFP+ macrophage number in the head at 2 dpf (n=6). Mean ± SEM of the GFP$^+$ macrophage numbers are shown.

Supp Fig 3. related to Fig. 3 and 4. Ontogenetically distinct macrophages recruitment after tail injury at different developmental stages.

(A) Tail fin of *Tg(fli1a:creERT2;mpeg1:Switch)* were amputated at 2 dpf and macrophage recruitment to the site of injury was analyzed. Representative images are shown at 48 hpa. Scale bar: 100µm.

(B) Tail fin of *Tg(fli1a:creERT2;mpeg1:Switch)* were amputated at 5 dpf and macrophage recruitment to the site of injury was analyzed. Representative images are shown at 48 hpa. Scale bar: 100µm.

(C) Switched *Tg(fli1a:creERT2;mpeg1:Switch)* larvae were treated with DMSO as a control, or metronidazole (MTZ) to ablate definitive macrophages. Treatments were performed from 4 to 6 dpf. Representative images are shown at 6 dpf. Scale bars: 100 µm.

(D) Quantification of DsRed and GFP macrophage number in the tail region 48 hours after DMSO (n=9) or MTZ treatments (n=9). Mean ± SEM of the DsRed$^+$ and GFP$^+$ macrophage numbers are shown. ****p ≤ 0.0001.

(E) Switched *Tg(fli1a:creERT2;mpeg1:Switch)* larvae were treated with DMSO or MTZ. Treatments were performed from 4 to 6 dpf and tail fins were amputated at 5 dpf. Representative images are shown 72 hpa. Scale bars: 100 µm.

(F) Cell proliferation was measured by EdU assay at 72 hpa. Red dots represent EdU$^+$ cells. Representative images are shown at 72 hpa of larvae treated with DMSO as a control, or metronidazole (MTZ) to ablate definitive macrophages. Scale bar: 100µm.

(G) Numbers of EdU$^+$ cells in switched *Tg(fli1a:creERT2;mpeg1:Switch)* larvae that were treated with DMSO (n=8) or MTZ (n=7). Unpaired t-test with Welch's correction was used for the analysis.